

# Time Series Alignment with Global Invariances

Titouan Vayer<sup>1 2</sup> Laetitia Chapel<sup>1 2</sup> Nicolas Courty<sup>1 2</sup> Rémi Flamary<sup>3</sup> Yann Soullard<sup>4 5 2</sup>  
Romain Tavenard<sup>4 5 2</sup>

## Abstract

In this work we address the problem of comparing time series while taking into account both feature space transformation and temporal variability. The proposed framework combines a latent global transformation of the feature space with the widely used Dynamic Time Warping (DTW). The latent global transformation captures the feature invariance while the DTW (or its smooth counterpart soft-DTW) deals with the temporal shifts. We cast the problem as a joint optimization over the global transformation and the temporal alignments. The versatility of our framework allows for several variants depending on the invariance class at stake. Among our contributions we define a differentiable loss for time series and present two algorithms for the computation of time series barycenters under our new geometry. We illustrate the interest of our approach on both simulated and real world data.

## 1. Introduction

Learning under distribution shift is one paradigm of major interest in the machine learning literature. Indeed, the training and the test data are often subject to collection bias (Torralba & Efros, 2011) or can be collected under heterogeneous conditions, because of different times of measurement, contexts or even measurement modalities (e.g. when different sensors are used to measure related quantities). In this setting, when it comes to generalize to out-of-distribution samples, machine learning algorithms are notoriously weak (Ben-David et al., 2010) as they rely on the correlations that are found in the training data (Arjovsky et al., 2019). Dedicated paradigms such as domain adaptation (Kouw & Loog, 2019), directly take into account this problem in the learning process. One other approach is

to learn, based on some prior knowledge, *w.r.t* some invariance classes in order to be more robust to irrelevant features transformations (Battaglia et al., 2018; Goodfellow et al., 2009). In this work, we aim at tackling this problem in the time series context through the definition of similarity measures that naturally encode desirable invariances. More precisely, we introduce similarity measures that are able to deal with both temporal and feature space transformations.

There exists many frameworks to register different spaces under some classes of invariance. In the shape analysis community, matching objects under rigid transformations is a widely-studied problem. Iterative Closest Point (ICP, Chen & Medioni (1992)) is a standard algorithm for such a task. It acts by alternating two simple steps: (i) matching points using nearest neighbor search and (ii) registering shapes together based on the obtained matches, which is known as the orthogonal Procrustes problem and has a closed form solution (Goodall, 1991). An extension of this algorithm presented in Alvarez-Melis et al. (2019a) uses optimal transport to match points at the first step, and it has been recently adapted to tree objects by considering a dedicated invariance class for the registration step (Alvarez-Melis et al., 2019b).

In the time series context, in order to deal with both local and global temporal distortions, a similarity measure called Dynamic Time Warping (DTW, Sakoe & Chiba (1978)) has been introduced. It is invariant (up to sampling artefacts) to any monotonically increasing temporal map that would align starting and end times. It has been initially introduced for speech processing applications and is now widely used in a variety of contexts such as human activity recognition (Chang et al., 2019), satellite image analysis (Wegner Maus et al., 2019) or medical applications (Huang & Lu, 2020). In this work, we aim at tackling both temporal and feature space invariances. To do so, we state the problem as a joint optimization over temporal alignments and feature space transformations, as depicted in Figure 1. That general framework allows the use of either DTW or its smoothed counterpart softDTW as an alignment procedure. Similarly, though rigid transformations of the feature space seem a reasonable invariance class, we show that our method can be used in conjunction with other families of transformations. Such a framework allows considering the case when time series differ both in length and feature space dimension-

<sup>1</sup>Université de Bretagne Sud, Vannes, France <sup>2</sup>UMR IRISA, Rennes, France <sup>3</sup>Université Côte d’Azur, Nice, France <sup>4</sup>Université de Rennes, Rennes, France <sup>5</sup>UMR LETG, Rennes, France. Correspondence to: Romain Tavenard <romain.tavenard@univ-rennes2.fr>.

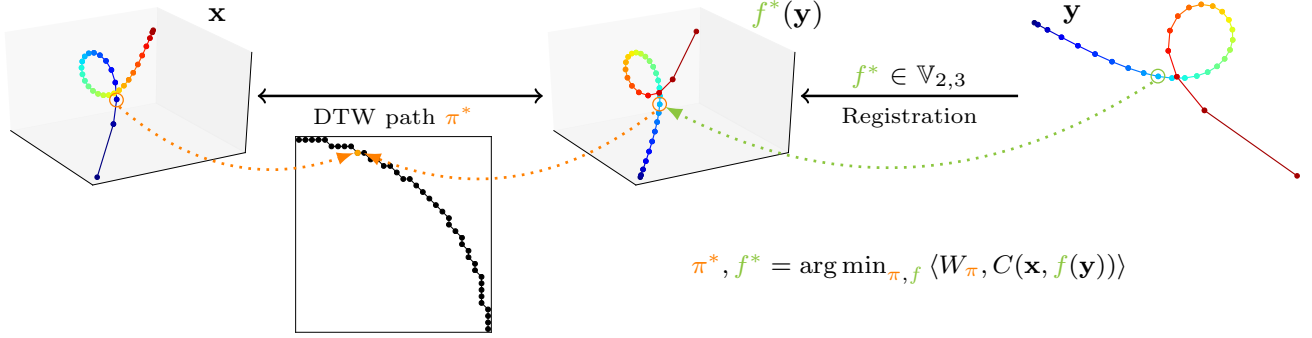


Figure 1. DTW-GI aligns time series by optimizing on temporal alignment (through Dynamic Time Warping) and feature space transformation (denoted  $f$  here). Time series represented here are color-coded trajectories, whose starting (resp. end) point is depicted in blue (resp. red).

ality. We introduce two different optimization procedures that could be used to tackle this problem and show experimentally that they lead to effectively invariant similarity measures. Our method can also be used to compute meaningful barycenters even when time series at stake do not lie in the same feature space. Finally, we showcase the versatility of our method and the importance to jointly learn feature space transformations and temporal alignments on two real-world applications that are time series forecasting for human motion and cover song identification.

## 2. Dynamic Time Warping (DTW)

Dynamic Time Warping (DTW, Sakoe & Chiba (1978)) is an algorithm used to assess similarity between time series, with extensions to multivariate time series proposed in (Ten Holt et al., 2007; Wöllmer et al., 2009). In its standard form, given two multivariate time series  $\mathbf{x} \in \mathbb{R}^{T_x \times p}$  and  $\mathbf{y} \in \mathbb{R}^{T_y \times p}$  of the same dimensionality  $p$ , DTW is defined as:

$$\text{DTW}(\mathbf{x}, \mathbf{y}) = \min_{\pi \in \mathcal{A}(\mathbf{x}, \mathbf{y})} \sum_{(i,j) \in \pi} d(\mathbf{x}_i, \mathbf{y}_j) \quad (1)$$

where  $\mathcal{A}(\mathbf{x}, \mathbf{y})$  is the set of all admissible alignments between  $\mathbf{x}$  and  $\mathbf{y}$  and  $d$  is a ground metric. In most cases,  $d$  is the squared Euclidean distance, i.e.  $d(\mathbf{x}_i, \mathbf{y}_j) = \|\mathbf{x}_i - \mathbf{y}_j\|^2$ .

An alignment  $\pi$  is a sequence of pairs of time frames which is considered to be admissible iff (i) it matches first (and respectively last) indexes of time series  $\mathbf{x}$  and  $\mathbf{y}$  together, (ii) it is monotonically increasing and (iii) it is connected (i.e. every index from one time series must be matched with at least one index from the other time series). Efficient computation of the above-defined similarity measure can be performed in quadratic time using dynamic programming,

relying on the following recurrence formula:

$$\begin{aligned} \text{DTW}(\mathbf{x}_{\rightarrow t_1}, \mathbf{y}_{\rightarrow t_2}) &= d(\mathbf{x}_{t_1}, \mathbf{y}_{t_2}) \\ &+ \min \begin{cases} \text{DTW}(\mathbf{x}_{\rightarrow t_1}, \mathbf{y}_{\rightarrow t_2-1}) \\ \text{DTW}(\mathbf{x}_{\rightarrow t_1-1}, \mathbf{y}_{\rightarrow t_2}) \\ \text{DTW}(\mathbf{x}_{\rightarrow t_1-1}, \mathbf{y}_{\rightarrow t_2-1}) \end{cases} \quad (2) \end{aligned}$$

Many variants of this similarity measure have been introduced. For example, the set of admissible alignment paths can be restricted to those lying around the diagonal using the so-called Itakura parallelogram or Sakoe-Chiba band, or a maximum path length can be enforced (Zhang et al., 2017). Most notably, a differentiable variant of DTW, coined soft-DTW, has been introduced in Cuturi & Blondel (2017) and is based on previous works on alignment kernels (Cuturi et al., 2007). It replaces the min operation in Equation (2) by a soft-min operator  $\min^\gamma$  whose smoothness is controlled by a parameter  $\gamma > 0$ , resulting in the  $\text{DTW}_\gamma$  distance:

$$\begin{aligned} \text{DTW}_\gamma(\mathbf{x}, \mathbf{y}) &= \min_{\pi \in \mathcal{A}(\mathbf{x}, \mathbf{y})}^\gamma \sum_{(i,j) \in \pi} d(\mathbf{x}_i, \mathbf{y}_j) \quad (3) \\ &= -\gamma \log \left( \sum_{\pi \in \mathcal{A}(\mathbf{x}, \mathbf{y})} e^{-\sum_{(i,j) \in \pi} d(\mathbf{x}_i, \mathbf{y}_j) / \gamma} \right). \end{aligned}$$

In the limit case  $\gamma = 0$ ,  $\min^\gamma$  reduces to a hard min operator and  $\text{DTW}_\gamma$  is defined as equivalent to the DTW algorithm.

## 3. DTW with Global Invariances

Despite their widespread use, DTW and softDTW are not able to deal with time series of different dimensionality or to encode feature transformations that may arise between time series. In the following, we introduce a new similarity measure aiming at aligning time series in this complex setting and provide ways to compute associated alignments. We also derive a Fréchet mean formulation that allows computing barycenters under this new geometry.

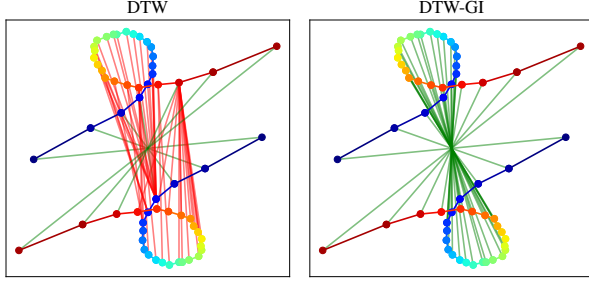


Figure 2. Example alignments between 2D time series (trajectories in the plane). Color coding corresponds to timestamps. Our DTW-GI method jointly estimates temporal alignment and global rotation between time series. On the contrary, standard DTW alignment fails at capturing feature space distortions and therefore produces mostly erroneous alignment (matching in red), except at the beginning and end of the time series, whose alignments are preserved thanks to DTW border constraints (cf. Section 2).

### 3.1. Definitions

Let  $\mathbf{x} \in \mathbb{R}^{T_x \times p_x}$  and  $\mathbf{y} \in \mathbb{R}^{T_y \times p_y}$  be two time series. In the following, we assume  $p_x \geq p_y$  without loss of generality. In order to allow comparison between time series  $\mathbf{x}$  and  $\mathbf{y}$ , we will optimize on a family of functions  $\mathcal{F}$  that map  $\mathbf{y}$  onto the feature space in which  $\mathbf{x}$  lies. More formally, we define Dynamic Time Warping with Global Invariances (DTW-GI) as the solution of the following joint optimization problem:

$$\text{DTW-GI}(\mathbf{x}, \mathbf{y}) = \min_{f \in \mathcal{F}, \pi \in \mathcal{A}(\mathbf{x}, \mathbf{y})} \sum_{(i,j) \in \pi} d(\mathbf{x}_i, f(\mathbf{y}_j)), \quad (4)$$

where  $\mathcal{F}$  is a family of functions from  $\mathbb{R}^{p_y}$  to  $\mathbb{R}^{p_x}$ . Note that this problem can also be written as:

$$\text{DTW-GI}(\mathbf{x}, \mathbf{y}) = \min_{f \in \mathcal{F}, \pi \in \mathcal{A}(\mathbf{x}, \mathbf{y})} \langle W_\pi, C(\mathbf{x}, f(\mathbf{y})) \rangle \quad (5)$$

where  $f(\mathbf{y})$  is a shortcut notation for the transformation  $f$  applied to all observations in  $\mathbf{y}$ ,  $\langle \cdot, \cdot \rangle$  denotes the Frobenius inner product,  $W_\pi$  is defined as:

$$\forall i \leq T_x, j \leq T_y, (W_\pi)_{i,j} = \begin{cases} 1 & \text{if } (i,j) \in \pi \\ 0 & \text{otherwise} \end{cases} \quad (6)$$

and  $C(\mathbf{x}, f(\mathbf{y}))$  is the cross-similarity matrix of squared Euclidean distances between samples from  $\mathbf{x}$  and  $f(\mathbf{y})$ , respectively. This definition can be extended to the softDTW case Equation (3) as proposed in the following:

$$\begin{aligned} \text{DTW}_\gamma\text{-GI}(\mathbf{x}, \mathbf{y}) &= \min_{f \in \mathcal{F}} \min_{\pi \in \mathcal{A}(\mathbf{x}, \mathbf{y})}^\gamma \langle W_\pi, C(\mathbf{x}, f(\mathbf{y})) \rangle \quad (7) \\ &= \min_{f \in \mathcal{F}} -\gamma \log \sum_{\pi \in \mathcal{A}(\mathbf{x}, \mathbf{y})} e^{-\langle W_\pi, C(\mathbf{x}, f(\mathbf{y})) \rangle / \gamma} \end{aligned}$$

Note that, due to the use of a soft-min operator, Equation (7) is no longer a joint optimization.

These similarity measures estimate both temporal alignment and feature space transformation between time series simultaneously, allowing the alignment of time series when the similarity should be defined up to a global transformation. For instance, one can see in Figure 2 two temporal alignments between two series in 2D that have been rotated in their feature space. In this case DTW-GI, whose invariant is the space of rotations, recovers the proper alignment whereas DTW fails.

**Properties of DTW-GI** By definition, DTW-GI and softDTW-GI are invariant under any global transformation  $T(\cdot)$  such that  $\{f \circ T \mid f \in \mathcal{F}\} = \mathcal{F}$  (i.e.  $\mathcal{F}$  is stable under  $T$ ), which motivates the names (soft)DTW with Global Invariances. It is also straightforward to see that  $\text{DTW-GI}(\mathbf{x}, \mathbf{x}) = 0$  for any time series  $\mathbf{x}$  as soon as  $\mathcal{F}$  contains the identity map.

### 3.2. Optimization

Optimization on the above-defined losses can be performed in several ways, depending of the nature of  $\mathcal{F}$ . We now present one optimization scheme for each loss.

#### 3.2.1. GRADIENT DESCENT

We first consider the optimization on the softDTW-GI loss in the case where  $\mathcal{F}$  is a parametric family of functions that are differentiable with respect to their parameters. Optimizing on problem (7) can be done with a gradient descent on the parameters of  $f$ . Since softDTW is smooth (contrary to DTW), this strategy can be used to compute gradients of  $\text{DTW}_\gamma\text{-GI}$  w.r.t. the parameter  $\theta$  of  $f_\theta$ . Complexity for this approach is driven by (i) that of a softDTW computation and (ii) that of computing  $f_\theta(\mathbf{y})$ . If we denote the latter  $c_f$ , overall complexity for this approach is hence  $O(n_{\text{iter}}(T_x T_y p_x + c_f))$ . Note that when Riemannian optimization is involved, an extra complexity term has to be added, corresponding to the cost of projecting gradients onto the considered manifold. This cost is  $O(p_y^3)$  for example when optimization is performed on the Stiefel manifold (Wen & Yin, 2013), which is an important case for our applications, as discussed in more details in the following.

#### 3.2.2. BLOCK COORDINATE DESCENT (BCD)

When DTW-GI is concerned, we introduce another strategy that consists in alternating minimization over (i) the temporal alignment and (ii) the feature space transformations in Equation (5). We will refer to this strategy as Block-Coordinate Descent (BCD) in the following.

Optimization over the alignment path given a fixed transformation  $f$  solely consists in a DTW alignment, as described in Section 2. For a fixed alignment path, the optimization

problem then becomes:

$$\min_{f \in \mathcal{F}} \langle W_\pi, C(\mathbf{x}, f(\mathbf{y})) \rangle. \quad (8)$$

Recall that  $C$  is a matrix of squared distances, which means that the problem above is a weighted least square problem. Depending on  $\mathcal{F}$ , there can exist a closed form solution for this problem (e.g. when  $\mathcal{F}$  is the set of affine maps with no further constraints). Let us first note that the matrix  $C$  can be rewritten as:

$$C(\mathbf{x}, f(\mathbf{y})) = \mathbf{u}_\mathbf{x} + \mathbf{v}_{f(\mathbf{y})}^T - 2\mathbf{x}f(\mathbf{y})^T \quad (9)$$

where  $\mathbf{u}_\mathbf{x} = (\|x_1\|^2, \dots, \|x_{T_x}\|^2)^T$  and  $\mathbf{v}_{f(\mathbf{y})} = (\|f(y_1)\|^2, \dots, \|f(y_{T_y})\|^2)^T$ . Note that the optimization problem reduces to the linear term on the right if  $\mathcal{F}$  is a set of norm preserving operations.

**Estimating  $f$  in the Stiefel manifold** Let us consider the case where  $\mathcal{F}$  is the set of linear maps whose linear operator is an orthonormal matrix, hence lying on the Stiefel manifold that we denote  $\mathbb{V}_{p_y, p_x}$  in the following. This invariance class encodes rigid transformations of the features. In this case, the optimization problem becomes:

$$\min_{\mathbf{P} \in \mathbb{V}_{p_y, p_x}} \langle W_\pi, \mathbf{u}_\mathbf{x} + \mathbf{v}_{f(\mathbf{y})}^T - 2\mathbf{x}\mathbf{P}\mathbf{y}^T \rangle \quad (10)$$

and we have  $\mathbf{v}_{f(\mathbf{y})} = (\|y_1\|^2, \dots, \|y_{T_y}\|^2)^T = \mathbf{v}_\mathbf{y}$  since the considered applications are norm-preserving. Overall, we get the following optimization problem:

$$\min_{\mathbf{P} \in \mathbb{V}_{p_y, p_x}} \langle W_\pi, \mathbf{u}_\mathbf{x} + \mathbf{v}_\mathbf{y}^T \rangle - 2 \langle W_\pi, \mathbf{x}\mathbf{P}\mathbf{y}^T \rangle \quad (11)$$

whose solution is equivalent to solving:

$$\max_{\mathbf{P} \in \mathbb{V}_{p_y, p_x}} \langle W_\pi, \mathbf{x}\mathbf{P}\mathbf{y}^T \rangle = \max_{\mathbf{P} \in \mathbb{V}_{p_y, p_x}} \langle \mathbf{x}^T W_\pi \mathbf{y}, \mathbf{P} \rangle \quad (12)$$

since the term  $\langle W_\pi, \mathbf{u}_\mathbf{x} + \mathbf{v}_\mathbf{y}^T \rangle$  does not depend in  $\mathbf{P}$ .

As described in Jaggi (2013), the latter problem can be solved exactly using Singular Value Decomposition (SVD): if  $U\Sigma V^T = M$  is the SVD of a matrix  $M$  of shape  $(p_y, p_x)$ , then  $S^* = UV^T$  is a solution to the linear problem  $\sup_{S \in \mathbb{V}_{p_y, p_x}} \langle S, M \rangle$ . Note that an extension of this method in the case where  $\mathcal{F}$  is an affine map whose linear part lies in the Stiefel manifold is straightforward, as discussed for example in Lawrence et al. (2019).

Interestingly, this optimization strategy where we alternate between time series alignment, *i.e.* time correspondences between both time series, and feature space transform optimization can be seen as a variant of the Iterative Closest Point (ICP) method in image registration (Chen & Medioni, 1992), in which nearest neighbors are replaced by matches

resulting from DTW alignment. Its overall complexity is then  $O(n_{\text{iter}}(T_x T_y p_x + p_x^2 p_y))$ . This complexity is equal to that of the gradient-descent when  $p_x = O(p_y)$ . However, in practice, the number of iterations required is much lower for this BCD variant, making it a very competitive optimization scheme, as discussed in Section 4.

### 3.3. Barycenters

Let us now assume we are given a set  $\{\mathbf{x}^{(i)}\}_i$  of time series of possibly different lengths and dimensionalities. A barycenter of this set in the DTW-GI sense is a solution to the following optimization problem:

$$\min_{\mathbf{b} \in \mathbb{R}^{T \times p}} \sum_i w_i \min_{f_i \in \mathcal{F}} DTW(\mathbf{x}^{(i)}, f_i(\mathbf{b})), \quad (13)$$

where weights  $\{w_i\}_i$  as well as barycenter length  $T$  and dimensionality  $p$  are provided as input to the problem. Note that, with this formulation, when  $\mathcal{F}$  is the Stiefel manifold,  $p$  is supposed to be lower or equal to the dimensionality of any time series in the set  $\{\mathbf{x}^{(i)}\}_i$ .

In terms of optimization, as for similarity estimation, two schemes can be used. First, softDTW-GI barycenters can be estimated through gradient descent (and when the set of series to be averaged is large, a stochastic variant relying on minibatches can easily be implemented). Second, when BCD is used for time series alignment, barycenters can be estimated using a similar approach as DTW Barycenter Averaging (DBA, Petitjean et al. (2011)), that would consist in alternating between barycentric coordinate estimation and DTW-GI alignments.

## 4. Experiments

In this section, we provide an experimental study of DTW-GI (and its soft counterpart) on simulated data and real-world datasets. Unless otherwise specified, the set  $\mathcal{F}$  of feature space transforms is the set of affine maps whose linear part lies in the Stiefel manifold. In all our experiments, tslearn (Tavenard et al., 2017) implementation is used for baseline methods and gradient descent on the Stiefel manifold is performed using GeoOpt (Kochurov et al., 2019; Becigneul & Ganeva, 2019) in conjunction with PyTorch. Open source code of our method will be released upon publication and is provided as supplementary material.

### 4.1. Timings

We are first interested in a quantitative evaluation of the temporal complexity of our methods. Note that the theoretical complexity of DTW and softDTW are the same, hence any difference observed in this series of experiments between DTW-GI and softDTW-GI would be solely due to their optimization schemes discussed in Section 3.2. In

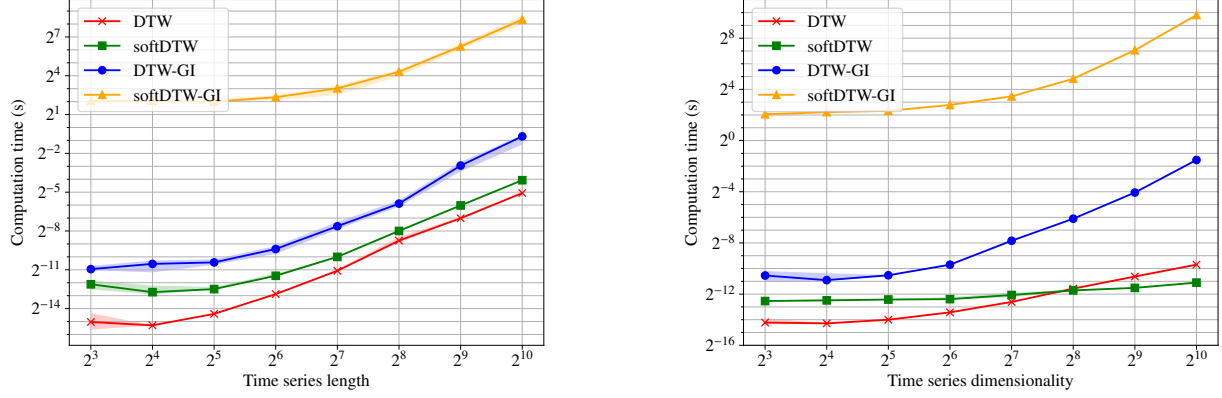


Figure 3. Computing time as a function of time series length (left) and dimensionality (right). Solid lines correspond to mean values and shaded areas correspond to 20th (resp. 80th) percentiles.

these experiments, the number of iterations for BCD as well as the number of gradient steps for the gradient descent optimizer are set to 5,000. The BCD algorithm used for DTW-GI is stopped as soon as it reaches a local minimum, while early stopping is used for the gradient-descent variant with a patience parameter set to 100 iterations.

We first study the computation time as a function of the length of the time series involved. To do so, we generate random time series in dimension 8 and vary their length from 8 to 1,024 timestamps. Figure 3 (left) shows a clear quadratic trend for all 4 methods presented. Note that DTW-GI and its BCD optimizer clearly outperform the gradient descent strategy used for softDTW-GI because the latter requires more iterations before early stopping can be triggered. Building on this, we now turn our focus on the impact of feature space dimensionality  $p$  (with a fixed time series length of 32). Baselines are asymptotically linear with respect to  $p$ . Since feature space registration is performed through optimization on the Stiefel manifold, both our optimization schemes rely on Singular Value Decomposition, which leads to an  $O(p^3)$  complexity that can also be observed for both methods in Figure 3 (right).

#### 4.2. Rotational invariance

We now evaluate the ability of our method to recover invariance to rotation. To do so, we rely on a synthetic dataset of noisy spiral-like 2d trajectories. For increasing values of an angle  $\theta$ , we generate pairs of spirals rotated by  $\theta$  with additive gaussian noise. Alignments between a reference time series and variants that are subject to an increasing rotation  $\theta$  are computed and repeated 50 times per angle. The ratio of each distance to the distance when  $\theta = 0$  is reported in Figure 4. One can clearly see that the GI counterparts of DTW and softDTW are invariant to rotation in the 2d feature space, while DTW and softDTW are not.

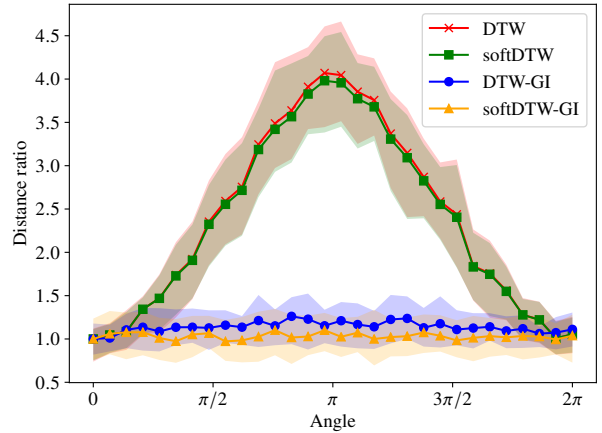


Figure 4. Illustration of the rotation invariance provided by DTW-GI. Mean distance ratios are reported as solid lines and shaded areas correspond to 20th (resp. 80th) percentiles.

#### 4.3. Barycenter computation

So as to better grasp the notion of similarity captured by our methods, we compute barycenters using the strategy presented in Section 3.3. Barycenters are computed for 3 different datasets: the first two are made of 2d trajectories of rotated and noisy spirals or folia, and the third one is composed of both 2- and 3-dimensional spirals (see samples in the left part of Figure 5). For each dataset, we provide barycenters obtained by two baseline methods. DTW Barycenter Averaging (DBA, [Petitjean et al. \(2011\)](#)) is used for DTW while softDTW resorts to a gradient-descent scheme to compute the barycenters. Their GI counterpart use the same algorithms but rely on the alignments obtained from DTW-GI and softDTW-GI respectively. Note that the baselines can-



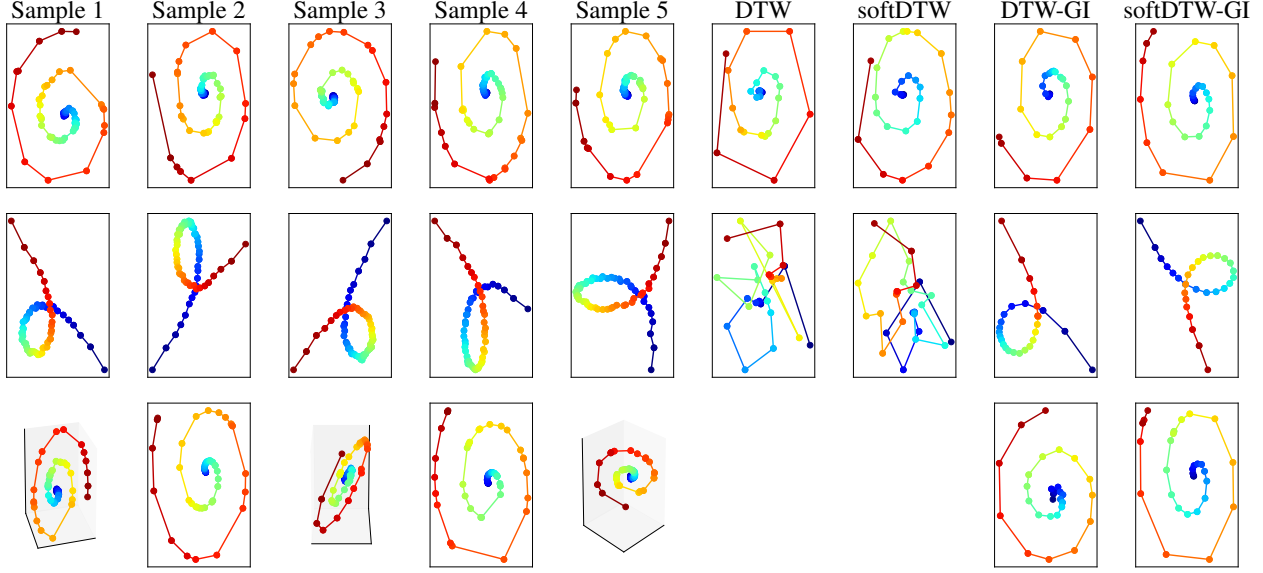


Figure 5. Barycenter computation using (i) DTW and softDTW baseline approaches, (ii) their rotation-invariant counterparts DTW-GI and softDTW-GI. Each row correspond to a different dataset, and the latter one contains both 2d and 3d trajectories, hence cannot be tackled by any baseline method. Trajectories are color-coded from blue (beginning of the series) to red (end of the series).

not be used for the third dataset since features of the time series do not lie in the same ambient space.

For the 2d spiral dataset, all the reconstructed barycenters can be considered as meaningful. This is because of the quasi-symmetries of the data at stake, that allows DTW and softDTW to recover sensible barycenters. Note however that the outer loop of the spiral (the one that suffers the most from the rotation) is better reconstructed using DTW-GI and softDTW-GI variants. When it comes to the folia trajectories, that are more impacted by rotations, baseline barycenters fail to capture the inherent structure of the trajectories at stake, while both our methods generate smooth and representative barycenters. DTW-GI and softDTW-GI are even able to recover barycenters when datasets are made of series that do not lie in the same space, as shown in the third row of Figure 5. Finally, in all three settings considered, temporal alignments successfully capture the irregular sampling from the samples to be averaged (denser towards the center of the spiral / loop of the folium).

#### 4.4. Time series forecasting

To further illustrate the benefit of our approach, we consider a time series forecasting problem (Le Guen & Thome, 2019), where the goal is to infer the future of a partial time series. In this setting, we suppose that we have access to a training set of full time series  $\mathbf{X}$ , with  $\mathbf{x}^{(i)} \in \mathbf{X}$  a time series of length  $T$  and dimensionality  $p$ , and another test set of partial time series  $\mathbf{Y}$  where each  $\mathbf{y} \in \mathbf{Y}$  is of length  $T' < T$

and dimensionality  $p$ . The goal is to predict the values for timestamps  $T'$  to  $T$  for each test time series. We will denote by  $\mathbf{x}_{\rightarrow T'}$  the beginning of the time series  $\mathbf{x}$  (up to time  $T'$ ) and  $\mathbf{x}_{T' \rightarrow}$  its end (from time  $T'$  to time  $T$ ).

Let  $d(\mathbf{y}, \mathbf{x}_i)$  denote a dissimilarity measure between time series  $\mathbf{y}$  and  $\mathbf{x}_i$  associated with a transformation  $f_i \in \mathcal{F} : \mathbb{R}^{p_x} \rightarrow \mathbb{R}^{p_y}$  that maps the features of  $\mathbf{x}_i$  onto the features of  $\mathbf{y}$ . This function aims at capturing the desired invariances in the feature space, as described in the previous section. A typical example is when  $d$  is the softDTW-GI cost, then the  $f_i$  are the Stiefel linear maps which capture the possible rigid transformation between the features. We propose to predict the future of a time series  $\mathbf{y}$  as follows:

$$\hat{\mathbf{y}}_{T' \rightarrow} = \sum_i a_d \left( \mathbf{y}_{\rightarrow T'}, \mathbf{x}_{\rightarrow T'}^{(i)} \right) f_i \left( \mathbf{x}_{T' \rightarrow}^{(i)} \right) \quad (14)$$

where  $a_d$  is the attention kernel:

$$a_d(\mathbf{y}, \mathbf{x}_i) = \frac{e^{-\lambda d(\mathbf{y}, \mathbf{x}_i)}}{\sum_j e^{-\lambda d(\mathbf{y}, \mathbf{x}_j)}} \quad (15)$$

with  $\lambda > 0$ . The prediction is based on the known timestamps for the time series of the training set and on transformations  $f_i$  that aim at capturing the latent transformation between training and test time series. The attention kernel gives more importance to time series that are close to the time series we want to forecast *w.r.t.* the notion of dissimilarity  $d$ . Note that for large values of  $\lambda$ , the softmax in Equation (15) converges to a hard max and the proposed approach corresponds to a nearest neighbor imputation.

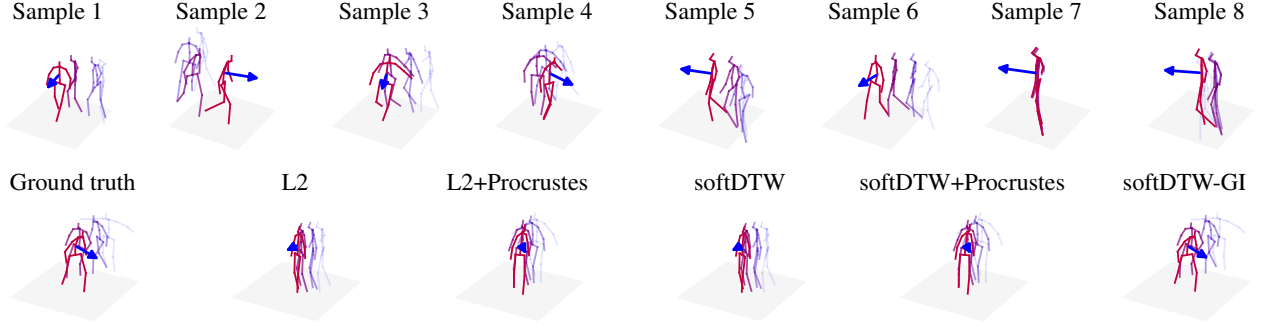


Figure 6. Examples of the forecasted subseries. Training samples  $\mathbf{x}_{T' \rightarrow}^{(i)}$  are depicted in top row while ground truth  $\mathbf{y}_{T' \rightarrow}$  and structured predictions  $\hat{\mathbf{y}}_{T' \rightarrow}$  are represented in bottom row. For each movement an arrow indicates the orientation of the subject. The beginning of the movement is displayed in shaded blue while the end is displayed in bold red.

$\lambda$	L2	L2+Procrustes	softDTW	softDTW+Procrustes	softDTW-GI
$10^{-3}$	98.24 +/- 1.14	16.50 +/- 1.25	75.41 +/- 0.90	16.46 +/- 1.24	12.34 +/- 0.65
$10^{-2}$	97.21 +/- 1.11	16.12 +/- 1.00	<b>65.39 +/- 0.69</b>	15.71 +/- 0.94	<b>8.30 +/- 1.26</b>
$10^{-1}$	83.65 +/- 0.74	<b>12.63 +/- 0.65</b>	65.39 +/- 0.69	<b>11.32 +/- 0.58</b>	13.41 +/- 1.05
$10^0$	<b>65.39 +/- 0.69</b>	19.62 +/- 1.17	65.39 +/- 0.69	19.96 +/- 0.91	17.61 +/- 2.23

Table 1. Average prediction loss on tests subjects with different values of  $\lambda$

**Dataset and methodology** We use the *Human3.6M* dataset (Ionescu et al., 2014) which consists of 3.6 million video frames of human movements recorded in a controlled indoor motion capture setting. This dataset is composed of 7 actors performing 15 activities (“Walking”, “Sitting” ...) twice. We are interested in forecasting the 3D positions of the subject joints evolving over time. We follow the same data partition as Coskun et al. (2017): the training set has 5 subjects (S1, S5, S6, S7 and S8) and the remaining 2 subjects (S9 and S11) compose the test set. In our experiments, we set the limit frames as  $T' = 100, T = 200$  which corresponds to predicting two seconds of movement given the previous two seconds. To emulate possible changes in signal acquisition (e.g. rotations of the camera), we randomly rotate the train subjects *w.r.t.* the  $z$ -axis. We consider the movements of type “Walking”, “WalkDog” and “Walk-Together” for the training set and “Walking” for the test set. Top row of Figure 6 illustrates samples of movements resulting from this procedure and the resulting dataset is provided as supplementary material.

**Competing structured prediction methods** Since our motions are in 3d, we look for global transformations of the features  $f_i : \mathbb{R}^3 \rightarrow \mathbb{R}^3$ . We use softDTW-GI as our similarity measure and its associated map  $f_i$  as described in Equation (7). We compare softDTW-GI to 5 baselines, that correspond to different pairs of time series similarity measure and feature space invariances. The first two baselines

do not encode any feature space invariance and are based on  $\ell_2$  and softDTW similarities respectively. They are denoted L2 and softDTW and use the identity map for all  $f_i$ . We also consider a *Procrustes* baseline (Goodall, 1991) defined as:

$$d(\mathbf{y}_{\rightarrow T'}, \mathbf{x}_{\rightarrow T'}^{(i)}) = \min_{\mathbf{P} \in \mathbb{V}_{3,3}, \mathbf{b} \in \mathbb{R}^3} \|(\mathbf{x}_{\rightarrow T'}^{(i)} \mathbf{P}^T + \mathbf{b}) - \mathbf{y}_{\rightarrow T'}\|_2^2 \quad (16)$$

The corresponding transformation  $f_i$  is the affine map based on the optimal  $\mathbf{P}^*, \mathbf{b}^*$  found by the previous problem. We denote this baseline L2+Procrustes. The last baseline is computed by first registering series using the Procrustes procedure defined above and then using the similarity measure  $d(\mathbf{y}_{\rightarrow T'}, \mathbf{x}_{\rightarrow T'}^{(i)}) = \text{DTW}_\gamma(\mathbf{y}_{\rightarrow T'}, \mathbf{x}_{\rightarrow T'}^{(i)} \mathbf{P}^{*T} + \mathbf{b}^*)$ . It is denoted as softDTW+Procrustes.

**Results** Qualitative and quantitative results are provided in Figure 6 and Table 1 respectively. We evaluate, for each test subject, the  $\ell_2$  reconstruction loss  $\|\mathbf{y}_{T' \rightarrow} - \hat{\mathbf{y}}_{T' \rightarrow}\|_2$  between the ground truth time series and its prediction. Table 1 displays the average loss on the test subjects for different values of the soft-max parameter  $\lambda \in \{10^{-3}, \dots, 10^0\}$ . Figure 6 presents examples of reconstructed movements.

In all cases we observe that softDTW and L2 lead to the worst reconstruction losses. Moreover, one can observe qualitatively that these methods struggle to cope with the difference in orientation of the subjects thus tending to shrink the prediction. On the contrary, by captur-

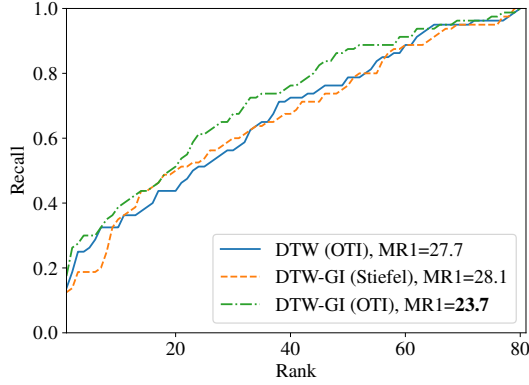


Figure 7. Cover song identification using the covers80 dataset. Methods are compared in terms of recall.

ing the possible spatial variability, `L2+Procrustes` and `softDTW+Procrustes` perform reasonably well but do struggle with the dynamics of the movement as shown in Figure 6. It can be explained by the fact that the optimal transformations found by the *Procrustes* analysis suppose a one-to-one correspondence of the points (*i.e.*  $y_{\rightarrow T'}(t)$  corresponds to  $x_{\rightarrow T'}^{(i)}(t)$  at time  $t$ ) and do not consider the temporal shifts between them. In this way, both methods lead to unrealistic transformations when the dynamics of movements are not the same. On the opposite, `softDTW-GI` method leads to the best results, highlighting the benefits of our approach over methods that either discard the temporal variability of the movements (`L2`, `L2+Procrustes`) or its spatial variability (`softDTW`). More importantly, the results advocate for a joint realignment of time and space since it leads to better results than a two-step procedure such as `softDTW+Procrustes` which first finds the feature transformation and then aligns series in time.

#### 4.5. Cover song identification

Cover song identification is the task of retrieving, for a given query song, its covers (*i.e.* different versions of the same song) in a training set. State-of-the-art methods either rely on anchor matches in the songs and/or on temporal alignments. In most related works, chroma or harmonic pitch class profile (HPCP) features are usually chosen, as they capture harmonic characteristics of the songs at stake (Heo et al., 2017).

For this experiment, we use the covers80 dataset (Ellis & Cotton, 2007) that consists in 80 cover pairs of pop songs and we evaluate the performance in terms of recall. Since the selection of features is not our main focus, we choose to extract chroma energy normalized statistics (CENS, Müller et al. (2005)) over half a second windows. We compare variants of our method to a baseline that consists in a DTW

alignment between songs transposed to the same key using the Optimal Transposition Index (OTI, Serra et al. (2008)). This OTI computes a transposition based on average energy in each semitone band. Note that we also compared our approach to the Smith Waterman algorithm in place of DTW but we chose to put it in supplementary material since it did not lead to significant improvement over the DTW baseline.

Figure 7 presents recall scores for compared methods as well as the mean rank of the first correctly identified cover (MR1) that is a standard evaluation metric for the task (used in MIREX<sup>1</sup> for example). Presented results show that DTW-GI with feature space optimization on the Stiefel manifold gets comparable results to the baseline. Interestingly enough, one can notice that the OTI strategy could be adapted to our context. Using the BCD optimization scheme, we are able to compute the optimal transposition index along the alignment path (instead of computing it on averaged features) at each iteration of the algorithm. This leads to a significant improvement of the performance and illustrates both the versatility of our method and the importance of performing joint feature space transformation and temporal alignment.

## 5. Conclusion and Perspectives

We propose in this paper a novel similarity measure that can compare time series across different spaces in order to tackle both temporal and feature space invariances. This work extends the well-known Dynamic Time Warping algorithm to deal with time series from different spaces thanks to the introduction of a joint optimization over temporal alignments and space transformations. In addition, we provide a formulation for the computation of the barycenter of a set of time series under our new geometry, which is, to the best of our knowledge, the first barycenter formulation for a set of heterogeneous time series. Another important special case of our approach allows for performing temporal alignment of time series with invariance to rotations in the feature space.

We illustrate our approach on several datasets. First, we use simulated time series to study the computational complexity of our approach and illustrate invariance to rotations. Then, we apply our approach on two real-life datasets for human motion prediction and cover song identification where invariant similarity measures are shown to improve performance.

Extension of this work will consider scenarios where features of the series do not lie in a Euclidean space, which would allow covering the case of structured data such as graphs evolving over time, for example. Future works also include the use of our methods in more elaborated models where, following ideas from Cai et al. (2019); Iwana et al.

<sup>1</sup>[https://www.music-ir.org/mirex/wiki/2019:Audio\\_Cover\\_Song\\_Identification](https://www.music-ir.org/mirex/wiki/2019:Audio_Cover_Song_Identification)



(2020), softDTW-GI could be used as a feature extractor in neural networks. It could also serve as a loss to train heterogeneous time series forecasting models (Le Guen & Thome, 2019; Cuturi & Blondel, 2017).

## References

- Alvarez-Melis, D., Jegelka, S., and Jaakkola, T. S. Towards optimal transport with global invariances. In *Proceedings of the International Conference on Artificial Intelligence and Statistics*, 2019a.
- Alvarez-Melis, D., Mroueh, Y., and Jaakkola, T. S. Un-supervised hierarchy matching with optimal transport over hyperbolic spaces. *arXiv preprint arXiv:1911.02536*, 2019b.
- Arjovsky, M., Bottou, L., Gulrajani, I., and Lopez-Paz, D. Invariant risk minimization. *arXiv preprint arXiv:1907.02893*, 2019.
- Battaglia, P., Hamrick, J. B. C., Bapst, V., Sanchez, A., Zambaldi, V., Malinowski, M., Tacchetti, A., Raposo, D., Santoro, A., Faulkner, R., Gulcehre, C., Song, F., Ballard, A., Gilmer, J., Dahl, G. E., Vaswani, A., Allen, K., Nash, C., Langston, V. J., Dyer, C., Heess, N., Wierstra, D., Kohli, P., Botvinick, M., Vinyals, O., Li, Y., and Pascanu, R. Relational inductive biases, deep learning, and graph networks. *arXiv*, 2018.
- Becigneul, G. and Ganea, O.-E. Riemannian adaptive optimization methods. In *Proceedings of the International Conference on Learning Representations*, 2019.
- Ben-David, S., Lu, T., Luu, T., and Pál, D. Impossibility theorems for domain adaptation. In *Proceedings of the International Conference on Artificial Intelligence and Statistics*, pp. 129–136, 2010.
- Cai, X., Xu, T., Yi, J., Huang, J., and Rajasekaran, S. Dtw-net: a dynamic time warping network. In *Neural Information Processing Systems*, pp. 11636–11646. Curran Associates, Inc., 2019.
- Chang, C.-Y., Huang, D.-A., Sui, Y., Fei-Fei, L., and Niebles, J. C. D3tw: Discriminative differentiable dynamic time warping for weakly supervised action alignment and segmentation. In *Proceedings of the IEEE Conference on Computer Vision and Pattern Recognition*, pp. 3546–3555, 2019.
- Chen, Y. and Medioni, G. Object modelling by registration of multiple range images. *Image and Vision Computing*, 10(3):145 – 155, 1992.
- Coskun, H., Achilles, F., DiPietro, R., Navab, N., and Tombari, F. Long short-term memory kalman filters: Recurrent neural estimators for pose regularization. In *Proceedings of the International Conference on Computer Vision*, Oct 2017.
- Cuturi, M. and Blondel, M. Soft-dtw: a differentiable loss function for time-series. In *Proceedings of the International Conference on Machine Learning*, pp. 894–903. JMLR. org, 2017.
- Cuturi, M., Vert, J.-P., Birkenes, O., and Matsui, T. A kernel for time series based on global alignments. In *Proceedings of the IEEE International Conference on Acoustics, Speech, and Signal Processing*, volume 2, pp. II–413. IEEE, 2007.
- Ellis, D. P. and Cotton, C. V. The 2007 labrosa cover song detection system. 2007.
- Goodall, C. Procrustes methods in the statistical analysis of shape. *Journal of the Royal Statistical Society: Series B (Methodological)*, 53(2):285–321, 1991.
- Goodfellow, I., Lee, H., Le, Q. V., Saxe, A., and Ng, A. Y. Measuring invariances in deep networks. In Bengio, Y., Schuurmans, D., Lafferty, J. D., Williams, C. K. I., and Culotta, A. (eds.), *Neural Information Processing Systems*, pp. 646–654. Curran Associates, Inc., 2009.
- Heo, H., Kim, H. J., Kim, W. S., and Lee, K. Cover song identification with metric learning using distance as a feature. In *Proceedings of the International Society for Music Information Retrieval Conference*, 2017.
- Huang, S.-F. and Lu, H.-P. Classification of temporal data using dynamic time warping and compressed learning. *Biomedical Signal Processing and Control*, 57:101781, 2020.
- Ionescu, C., Papava, D., Olaru, V., and Sminchisescu, C. Human3.6m: Large scale datasets and predictive methods for 3d human sensing in natural environments. *IEEE Transactions on Pattern Analysis and Machine Intelligence*, 36(7):1325–1339, jul 2014.
- Iwana, B., Frinken, V., and Uchida, S. Dtw-nn: A novel neural network for time series recognition using dynamic alignment between inputs and weights. *Knowledge-Based Systems*, 188, 1 2020. ISSN 0950-7051. doi: 10.1016/j.knosys.2019.104971.
- Jaggi, M. Revisiting frank-wolfe: Projection-free sparse convex optimization. In *Proceedings of the International Conference on Machine Learning*, 2013.
- Kochurov, M., Kozlukov, S., Karimov, R., and Yanush, V. Geoopt: Adaptive riemannian optimization in PyTorch, 2019. <https://github.com/geoopt/geoopt>.

- Kouw, W. M. and Loog, M. A review of domain adaptation without target labels. *IEEE Transactions on Pattern Analysis and Machine Intelligence*, 2019.
- Lawrence, J., Bernal, J., and Witzgall, C. A purely algebraic justification of the kabsch-umeyama algorithm. *Journal of Research of the National Institute of Standards and Technology*, 124:1–6, 2019.
- Le Guen, V. and Thome, N. Shape and time distortion loss for training deep time series forecasting models supplementary material. In *Neural Information Processing Systems*, 2019.
- Müller, M., Kurth, F., and Clausen, M. Audio matching via chroma-based statistical features. In *Proceedings of the International Society for Music Information Retrieval Conference*, 2005.
- Petitjean, F., Ketterlin, A., and Gançarski, P. A global averaging method for dynamic time warping, with applications to clustering. 44(3):678 – 693, 2011.
- Sakoe, H. and Chiba, S. Dynamic programming algorithm optimization for spoken word recognition. *IEEE Transactions on Acoustics, Speech and Signal Processing*, 26(1):43–49, 1978.
- Serra, J., Gómez, E., and Herrera, P. Transposing chroma representations to a common key. In *Proceeding sof the IEEE Conference on The Use of Symbols to Represent Music and Multimedia Objects*, pp. 45–48, 2008.
- Tavenard, R., Faouzi, J., Vandewiele, G., Divo, F., Androz, G., Holtz, C., Payne, M., Yurchak, R., Rußwurm, M., Kolar, K., and Woods, E. tslearn: A machine learning toolkit dedicated to time-series data, 2017. <https://github.com/rtavenar/tslearn>.
- Ten Holt, G. A., Reinders, M. J., and Hendriks, E. Multi-dimensional dynamic time warping for gesture recognition. In *Annual conference of the Advanced School for Computing and Imaging*, volume 300, pp. 1, 2007.
- Torralba, A. and Efros, A. A. Unbiased look at dataset bias. In *Proceedings of the IEEE Conference on Computer Vision and Pattern Recognition*, pp. 1521–1528, 2011.
- Wegner Maus, V., Câmara, G., Appel, M., and Pebesma, E. dtwsat: Time-weighted dynamic time warping for satellite image time series analysis in R. *Journal of Statistical Software*, 88(5):1–31, 2019.
- Wen, Z. and Yin, W. A feasible method for optimization with orthogonality constraints. *Mathematical Programming*, 142(1-2):397–434, 2013.
- Wöllmer, M., Al-Hames, M., Eyben, F., Schuller, B., and Rigoll, G. A multidimensional dynamic time warping algorithm for efficient multimodal fusion of asynchronous data streams. *Neurocomputing*, 73(1-3):366–380, 2009.
- Zhang, Z., Tavenard, R., Bailly, A., Tang, X., Tang, P., and Corpetti, T. Dynamic time warping under limited warping path length. *Information Sciences*, 393:91–107, 2017.

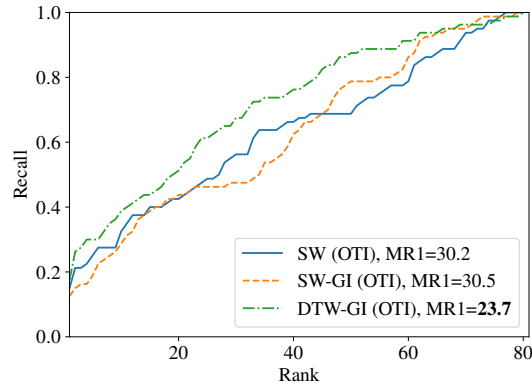


Figure 8. Cover song identification using the covers80 dataset. Methods are compared in terms of recall.

### A. An Extra Cover Song Identification Experiment

In section 4.5, we have experimented using Dynamic Time Warping as the base metric to align time series. Smith-Waterman algorithm can also be used for this task. We show in Figure 8 that our method applied to DTW with key transposition along the alignment (denoted “DTW-GI (OTI)”) outperforms both its Smith-Waterman counterpart and a baseline that would use Smith-Waterman in conjunction with pre-processing step based on OTI.